Title
Effect of excess lithium in LiMn2O4 and Li1.15Mn1.85O4 electrodes revealed by quantitative analysis of soft X-ray absorption spectroscopy

Journal
Applied Physics Letters, 110(9)

ISSN
0003-6951

Authors
Zhuo, Zengqing
Olalde-Velasco, Paul
Chin, Timothy
et al.

Publication Date
2017-02-27

DOI
10.1063/1.4977502

Peer reviewed

Effect of excess lithium in $LiMn_2O_4$ and $Li_{1.15}Mn_{1.85}O_4$ electrodes revealed by quantitative analysis of soft X-ray absorption spectroscopy

Zengqing Zhuo,[1,2] Paul. Olalde-Velasco,[2,a)] Timothy Chin,[3] Vincent Battaglia,[3] Stephen J. Harris,[2] Feng Pan, [1*] and Wanli Yang [2 *]

[1] *School of Advanced Materials, Peking University, Shenzhen Graduate School, Shenzhen 518055, People's Republic of China*

[2] *Advanced Light Source, Lawrence Berkeley National Laboratory, 1 Cyclotron Road, Berkeley CA 94720, United States*

[3] *Environmental Energy Technologies Division, Lawrence Berkeley National Laboratory, 1 Cyclotron Road, Berkeley CA 94720, United States*

We performed a comparative study of the soft x-ray absorption spectroscopy of the $LiMn_2O_4$ and $Li_{1.15}Mn_{1.85}O_4$ electrode materials with a quantitative analysis of the Mn oxidation states. The revealed redox evolution of Mn upon the electrochemical cycling clarifies the effect of the excess Li in the materials, which naturally explains the different electrochemical performance. The spectral analysis perfectly agrees with the different initial cycling capacities of the two materials. The results show unambiguously that Mn^{3+} starts to dominate the electrode surface after only one cycle. More importantly, the data show that, while $LiMn_2O_4$ electrodes follow the nominal Mn redox evolution, the formation of Mn^{3+} on the electrode surface is largely retarded for the $Li_{1.15}Mn_{1.85}O_4$ during most of the electrochemical process. Such a different surface Mn redox behavior leads to differences in the detrimental effects of Mn^{2+} formation on the surface, which is observed directly after only two cycles. Our results provide strong evidence that a key effect of the (bulk) excess Li doping is actually due to processes on the electrode surfaces.

Lithium ion batteries (LIBs) have become one of the most important energy storage technologies powering portable electronic devices and electric vehicles.[1] Compared with the first generation Co based layered compounds, the spinel $LiMn_2O_4$ (LMO) is an especially promising cathode material for LIBs due to its low cost, environmentally benign chemistry, thermal stability, and excellent rate performance.[2,3,4] However, capacity fading, or low capacity retention, remains a technical challenge for the commercial use of LMO. The issue is largely related to the evolution of Mn oxidation states during electrochemical cycling, which has been attributed to a number of factors, such as Jahn-Teller distortion of the Mn^{3+} phase,[5]

Mn^{2+} dissolution into the electrolyte,[6] and loss of crystalinity.[7] Due to the disproportionation reaction of Mn^{3+}, Mn^{2+} could form on the surface of LMO, especially in the presence of organic electrolyte solutions under high potential.[2,5,8] The dissolution of Mn^{2+}, mainly associated with the presence of an acidic electrolyte,[9] leads to the loss of active materials, and it is considered to be the main reason to capacity fade.[10] In general, it is widely believed that the problem of LMO electrodes stems from Mn species with specific valence values that are formed through either electrochemical cycling or surface reactions. Therefore, a detailed and quantitative study of the Mn valence evolution is critical for understanding the failure mode of LMO electrodes.

Doping the LMO materials by replacing Mn with low valence cations have been studied extensively. The hope is based on the stoichiometric consideration that Mn could be maintained at the desired high valence by doping with low-valence cations, so the detrimental Mn^{3+} and Mn^{2+} species could be suppressed. Among the various approaches, Li-rich $Li_{1+x}Mn_{2-x}O_4$ ($0<x<0.33$), i.e., doping with Li, has been demonstrated to suppress dissolution and reduce capacity fade, but with sacrificed capacity.[2,4,9,11] However, apart from general speculations based on the stoichiometry, there has been no experimental clarification on the excess Li-doping effect to explain the electrochemical performance.

In this study, we provide soft X-ray spectroscopic results for two LMO systems, $Li_{1.15}Mn_{1.85}O_4$ and $LiMn_2O_4$, with and without the excess Li doping respectively, at different electrochemical states. We found that excess Li doping effectively suppresses the Mn^{3+} and Mn^{2+} formation on the surface of the electrode. This information clarifies a key effect of excess Li and provides useful information for material optimization.

Soft X-ray absorption spectroscopy (sXAS) is a modern synchrotron based technique, providing information on key electronic states in the vicinity of Fermi level.[12] sXAS has been demonstrated to be a powerful tool to study LIB materials, especially for transition-metal (TM) oxide based cathode materials.[8,13,14] sXAS is a direct measurement of the TM *3d* states with high elemental, chemical and orbital sensitivity through the dipole-allowed *2p* to *3d* transitions. Quantitative analysis of TM *L*-edge sXAS, such as Fe[15-17], Mn[8,13,17] and Ni[18], provides detailed information about valence,[13,16] spin states,[15] and local structural effects[15,16,19], of battery materials[20]. In particular, we have demonstrated that quantitative analysis of the Mn valence distribution can be achieved reliably through a very straightforward linear combination fitting of the sXAS data of battery electrodes[8,13,17].

$LiMn_2O_4$ and $Li_{1.15}Mn_{1.85}O_4$ cathodes were prepared using commercial materials from EMI/Merck and TODA chemical companies, respectively. The preparation and characterization of the $LiMn_2O_4$ and $Li_{1.15}Mn_{1.85}O_4$ electrodes is standard and provided in the **supplementary material**. The raw powders, referred to as "pristine" samples in this paper, were compressed

to form a pellet inside an Ar glove box. Battery coin cells were prepared following standard procedure using Al metal electrodes. The cells were cycled at 0.1C rate and stopped at 1/3, 2/3, and fully delithiated (charged) levels during both the charging and discharging process for sXAS experiments. A typical electrochemical performance is shown in the supplementary materials (Figure S1). It is clear that the excess Li doping in $Li_{1.15}Mn_{1.85}O_4$ reduces the overall cycling capacity while greatly improving the capacity retention.

sXAS is performed at the Advanced Light Source's undulator beamline 8.0.1 of the Lawrence Berkeley National Laboratory. Its spherical grating monochromator delivers 10^{12} photons/second with linear polarization with a resolving power up to 6000[21]. The experimental resolution of the data presented in this work is 0.15 eV without considering the intrinsic core-hole broadening. Mn $L_{2,3}$ XAS measurements were collected at room temperature using the surface-sensitive total electron yield (TEY) mode by measuring the sample drain current with a surface probe depth of about 10 nm. All spectra have been normalized to the photon flux recorded by a clean gold mesh upstream of the experimental chamber. The raw spectra (Fig. S2 and S3) are normalized using the conventional background edge jump of the regions well below and beyond the L_3 and L_2 absorption edges, respectively. For quantitative fitting, a polynomial background was fitted and subtracted from the raw spectra to emphasize the features related to oxidation states.

FIG 1(a) and **FIG 2(a)** show the Mn L_3-edge sXAS results (solid lines) and the fits (dotted lines) for $LiMn_2O_4$ and $Li_{1.15}Mn_{1.85}O_4$ electrodes that are electrochemically cycled to the desired state-of-charge (SOC), as marked in **Fig. 1(b)** and **Fig. 2(b)**, respectively. Here, we focus on the Mn L_3-edge sXAS lineshape which is sensitive to the different chemical configurations and oxidation states[14]. For comparison purposes, the spectra from pristine powder and materials soaked in HCl acid are plotted on top. Quantitative fits and analyses of the evolution of the Mn oxidation states is obtained by fitting the experimental data using a linear combination of three reference spectra of $Mn^{2+}(MnO)$, $Mn^{3+}(Mn_2O_3)$, and $Mn^{4+}(MnO_2)$, as shown on the bottom[8,13,17]**.** Due to the difficulty of obtaining reliable Mn^{2+} spectra, which is sensitive not only to the oxidation state but also to the different surface phases,[22] the spectrum of Mn^{2+} was taken from our previous study,[14] which is consistent with the other work.[23] The fitting results (dotted lines in **FIG 1(a)** and **FIG 2(a)**) almost perfectly replicate the experimental data, validating this simple method of quantitative analysis. The fitted values of the Mn oxidation state concentrations are plotted in **FIG 1(c)** and **FIG 2(c)** for $LiMn_2O_4$ and $Li_{1.15}Mn_{1.85}O_4$, respectively.

First, for the pristine $LiMn_2O_4$ and $Li_{1.15}Mn_{1.85}O_4$ materials, the theoretical distribution of $Mn^{3+/4+}$ is 50%:50% (1:1) and 30%:70% (0.55:1.3) based on the stoichiometric estimation with Li^{1+} and O^{2-}. Our fitting values ("P" in **FIG 1(c)** and **FIG 2(c)**) are 47%:53% and 30%:70% for $LiMn_2O_4$ and $Li_{1.15}Mn_{1.85}O_4$, respectively. These values are in excellent agreement with

the theoretical estimation, and indicate the high precision of this simple fitting method for quantitative analysis. As shown in the cycling profiles in **Fig 1(b)** and **Fig 2(b)**, the first charge capacities of $LiMn_2O_4$ and $Li_{1.15}Mn_{1.85}O_4$ are 146 mAh g^{-1} and 94 mAh g^{-1} at 0.1C, respectively. The capacity ratio, 146:94 = 1.55, is again in perfect agreement with our fitting results of the Mn^{3+} content, 47:30 = 1.57, which justifies this fitting method and confirms that the initial electrochemical capacity is determined by the Mn^{3+} content in the pristine material.

Second, the spectra of both $LiMn_2O_4$ and $Li_{1.15}Mn_{1.85}O_4$ soaked with HCl solution show the lineshape of pure Mn^{4+} at the top of **Fig 1(a)** and **Fig 2(a)**. The effect of acid on $LiMn_2O_4$ in HCl solution has been studied before. The Mn^{3+} present in $LiMn_2O_4$ undergoes disproportionation to Mn^{2+} and Mn^{4+} when exposed to acid: $2LiMn_2O_4(s) + 4H^+(aq) \rightarrow 3MnO_2(s) + Mn^{2+}(aq) + 2Li^+(aq) + 2H_2O(aq)$.[9,24] Our sXAS spectra indicate that the excess Li doping in spinel electrode materials shows negligible effect in the term of the surface reactions with acid.

Third, we now focus on the Mn oxidation state evolution at different stages of the electrochemical cycling and the surprising contrast between the $LiMn_2O_4$ and $Li_{1.15}Mn_{1.85}O_4$ electrodes. Overall, the Mn L_3 sXAS lineshape evolves with electrochemical cycling for both $LiMn_2O_4$ and $Li_{1.15}Mn_{1.85}O_4$. In **FIG 1(a)**, for the $LiMn_2O_4$ electrodes, the intensity of the Mn^{3+} features around 641.3eV decreases with the charge (delithiation) progress, suggesting that the Mn valence changes from Mn^{3+} to Mn^{4+} during the charging process. During discharge, the sXAS lineshape is reversed gradually corresponding to the lithiation level, i.e., the lineshape of 1/3 (Dis) and 2/3 (Dis) are equivalent to the 1/3 (Cha) and 2/3 (Cha), respectively. Because sXAS is a surface probe, this gradual recovery of sXAS lineshape indicates that the surface oxidation state of Mn in $LiMn_2O_4$ more or less follows the general lithiation/delithiation process during the electrochemical operation. It is important to note that the contribution from Mn^{3+} is dramatically higher on the fully discharged electrode surface after only one cycle, which can be easily seen by comparing the spectra of the discharged and pristine samples. This result will be discussed separately below.

Contrasting the gradual sXAS lineshape change that follows the nominal lithiation level of the $LiMn_2O_4$ electrodes, **FIG 2(a)**, however, displays sXAS spectra of 6 $Li_{1.15}Mn_{1.85}O_4$ electrodes, from pristine to the 1/3 (Dis), with very small lineshape change. Except for the finite amount of Mn^{3+} contribution around 641.3 and 640 eV, all these spectra of the 6 samples show Mn^{4+} features that dominate at 640.5 and 643 eV. This strongly indicates that Mn^{4+} dominates the surface of $Li_{1.15}Mn_{1.85}O_4$ before the electrode is fully discharged.

The quantitative fitting of each sXAS spectrum, again, perfectly reproduces the experimental data (dotted lines in **FIG.1(a)** and **FIG.2(a)**), and the fitting results are plotted in **FIG 1(c)** and **FIG 2(c)** for $LiMn_2O_4$ and $Li_{1.15}Mn_{1.85}O_4$ electrodes, respectively. The quantified results emphasize the aforementioned contrasts of the sXAS lineshape evolution in

the two systems. It can be seen that the concentrations of the Mn^{3+} and Mn^{4+} follow the nominal delithiation (charge) and lithiation (discharge) processes for the $LiMn_2O_4$ electrodes (**Fig. 1(c)**), while it remains relatively stable through most of the charge/discharge process for the $Li_{1.15}Mn_{1.85}O_4$ electrodes before the fully discharged state (**Fig.2(c)**). Such a trend of the quantitative fitting results is consistent with the overall sXAS lineshape evolution upon electrochemical cycling.

In the fully discharged stage, the lineshape of Mn^{3+} starts to dominate for both the $LiMn_2O_4$ and $Li_{1.15}Mn_{1.85}O_4$ electrodes. It is obvious that the concentration of Mn^{3+} is much higher than that of the pristine samples (**FIG 1** and **FIG 2**). Because both the pristine and fully discharged samples are expected to fully lithiated, the obviously different sXAS lineshape shows that there are dramatic chemical and structural changes on the surface of the spinel electrodes after only one charge-discharge cycle: Mn^{3+} species dominate the electrode surface at the discharged state.

The importance of Mn^{3+} and the detrimental Mn^{2+} on battery electrode surfaces has been extensively discussed[2,5,8]. In order to emphasize the surface evolution of the spinel materials with only limited number of electrochemical cycles, **FIG 3** shows a direct comparison of the Mn *L* edge sXAS between $LiMn_2O_4$ and $Li_{1.15}Mn_{1.85}O_4$ for pristine, discharged after 1cycle, and discharged after 2 cycles. The peak located at 640.1eV belongs to the Mn^{2+}. It can be seen that the electrode surface is dominated by the low-valence Mn species after one cycle, as discussed above. Furthermore, the relative intensity of the Mn^{2+} feature keeps increasing with electrochemical cycling for the $LiMn_2O_4$ electrodes, but remains negligible for the $Li_{1.15}Mn_{1.85}O_4$ system, showing a clear contrast between the discharged samples after two cycles. Therefore, our data show that the excess Li doping not only maintains the high-valence Mn through a large electrochemical cycling window, it also helps to surpress the low-valence Mn formation on the surface at deep lithiation levels.

In summary, we performed soft x-ray absorption spectroscopy and a quantitative analysis of the Mn oxidation states in $LiMn_2O_4$ and $Li_{1.15}Mn_{1.85}O_4$ electrodes upon electrochemical cycling. The analysis clearly shows the relationship between the initial capacity and the experimental ratio of $Mn^{3+/4+}$. More importantly, we found excess Li doping in the $Li_{1.15}Mn_{1.85}O_4$ leads to the high-valence Mn^{4+} dominated surface within a large electrochemical cycling window, and it also surpresses the formation of Mn^{2+} on the electrode surface. We believe such surface effects play an important role on regulating the different electrochemical performance of the two contrasting electrode systems, and provides useful information for further optimization.

See the supplementary material at [URL will be inserted by AIP] for a full description of the electrode preparation and the typical electrochemical profile of the two electrodes.

This work was supported by National Materials Genome Project (2016YFB0700600), Guangdong Innovation Team Project (No. 2013N080), and Shenzhen Science and Technology Research Grant (peacock plan KYPT20141016105435850). Advanced Light Source is supported by the Director, Office of Science, Office of Basic Energy Sciences, of the U.S. Department of Energy under Contract No. DE-AC02-05CH11231. SJH acknowledges support from the Assistant Secretary for Energy Efficiency, Vehicle Technologies Office of the U.S. Department of Energy (U.S. DOE) under the Advanced Battery Materials Research (BMR).

Corresponding Author: *panfeng@pkusz.edu.cn, and **wlyang@lbl.gov**

a) **Present address:** *Instituto de Física, Benemerita Universidad Autónoma de Puebla, Apdo. Postal J-48, Puebla, Puebla 72570, México*.

FIGURES

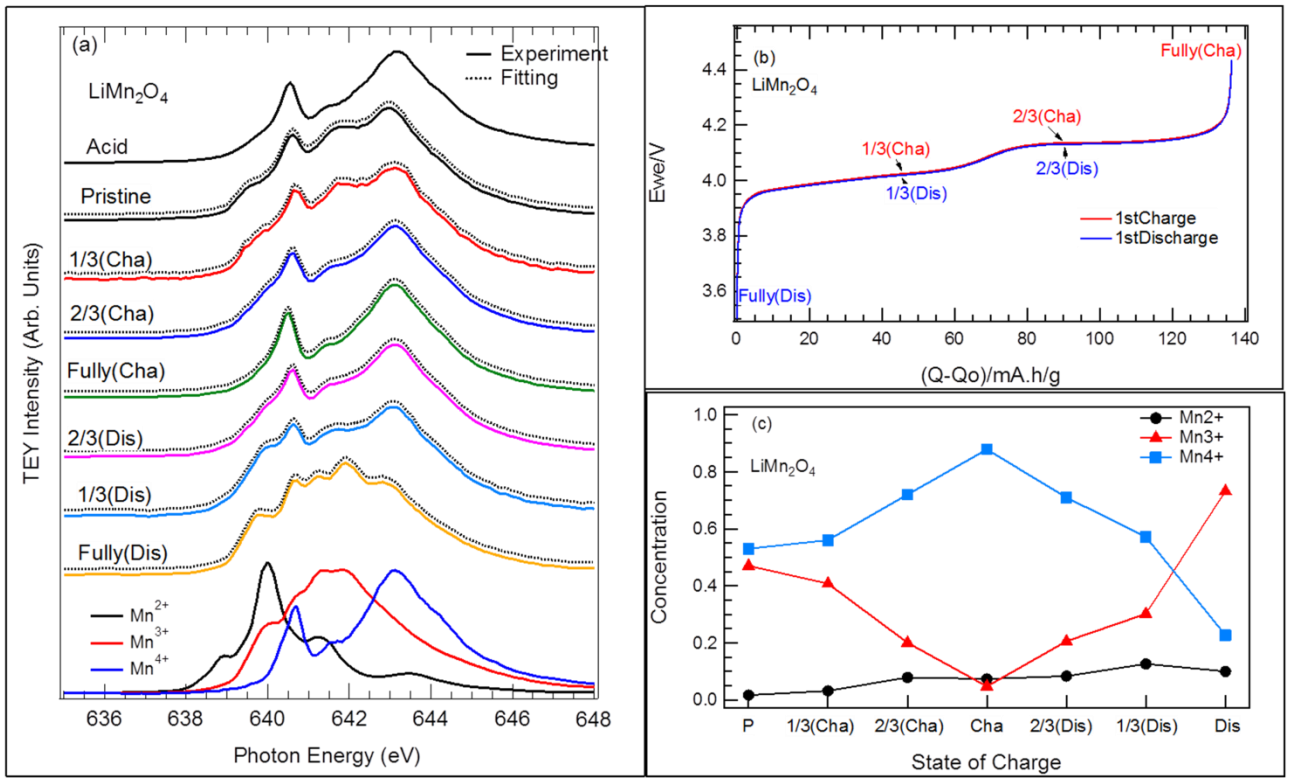

FIG. 1. (a) Mn L_3-edge sXAS spectra (solid line) of a series of $LiMn_2O_4$ electrodes, and the quantitative fitting (dotted line) through a simple linear combination of the reference spectra plotted on the bottom. The electrochemical status of the samples are marked in penal b). (b) The first charge and discharge profile at 0.1C with samples marked. (c) Fitting results of the Mn valence distribution at the corresponding SOC of $LiMn_2O_4$ electrodes.The samples are marked as the 1/3, 2/3, and fully delithiation (charged) levels during both the charging and discharging process.

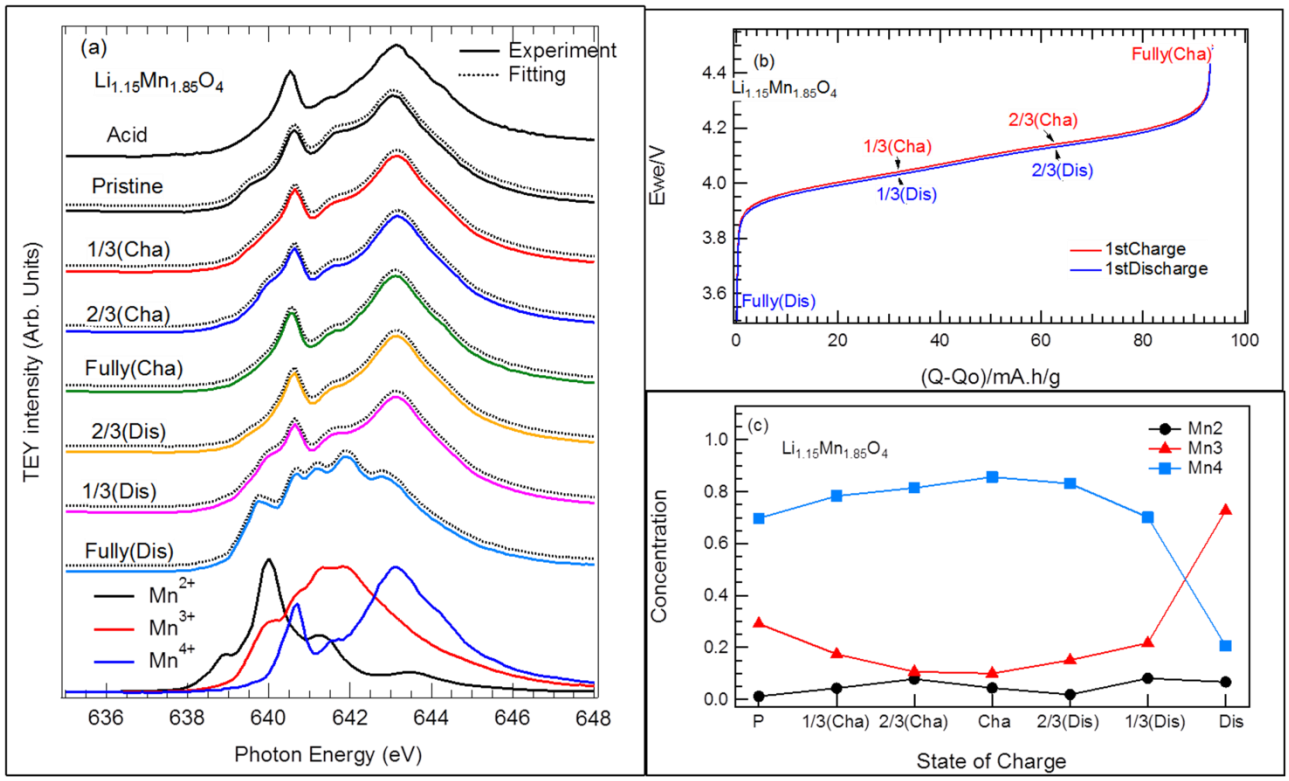

FIG. 2. (a) Mn L_3-edge sXAS spectra (solid line) of a series of $Li_{1.15}Mn_{1.85}O_4$ electrodes and the quantitative fittings (dotted line). (b) The first charge and discharge profile at 0.1C with samples marked. (c) Fitting results of the Mn valence distribution at the different SOC of $Li_{1.15}Mn_{1.85}O_4$.

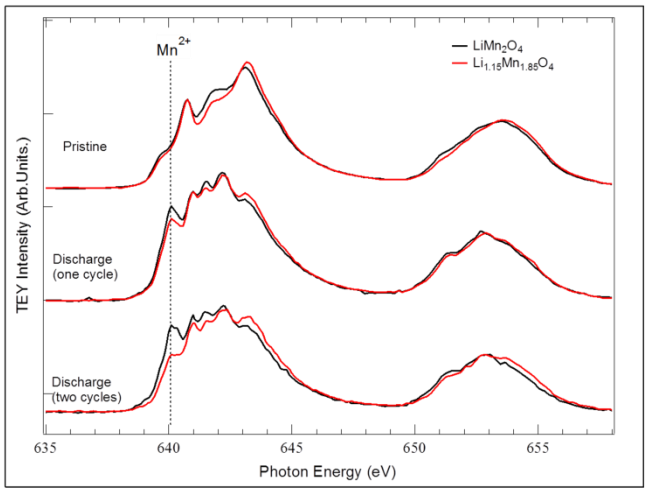

FIG. 3. Mn *L*-edge sXAS spectra of three sets of lithiated (discharged) $LiMn_2O_4$ (black) and $Li_{1.15}Mn_{1.85}O_4$ (red) samples.

1 John B. Goodenough and Kyu-Sung Park, J. Am. Chem. Soc. **135** (4), 1167 (2013); John B. Goodenough and Youngsik Kim, Chem. Mater. **22** (3), 587 (2010); Peter G. Bruce, Solid State Ionics **179** (21–26), 752 (2008); M. Armand and J. M. Tarascon, Nature **451** (7179), 652 (2008).

2 R. J. Gummow, A. de Kock, and M. M. Thackeray, Solid State Ionics **69** (1), 59 (1994).

3 Soo Kim, Muratahan Aykol, and C. Wolverton, Phys. Rev. B **92** (11), 115411 (2015); Matteo Bianchini, Emmanuelle Suard, Laurence Croguennec, and Christian Masquelier, J. Phys. Chem. C **118** (45), 25947 (2014); Joo-Seong Kim, KyungSu Kim, Woosuk Cho, Weon Ho Shin, Ryoji Kanno, and Jang Wook Choi, Nano Lett. **12** (12), 6358 (2012); R. Benedek and M. M. Thackeray, Phys. Rev. B **83** (19), 195439 (2011); Quan-Chao Zhuang, Tao Wei, Li-Li Du, Yong-Li Cui, Liang Fang, and Shi-Gang Sun, J. Phys. Chem. C **114** (18), 8614 (2010); J. M. Tarascon, E. Wang, F. K. Shokoohi, W. R. McKinnon, and S. Colson, J. Electrochem. Soc. **138** (10), 2859 (1991).

4 Michael M. Thackeray, Prog. Solid State Chem. **25** (1–2), 1 (1997).

5 Michael M. Thackeray, Yang Shao‐Horn, Arthur J. Kahaian, Keith D. Kepler, Eric Skinner, John T. Vaughey, and Stephen A. Hackney, Electrochem. Solid-State Lett. **1** (1), 7 (1998).

6 Dong H. Jang, Young J. Shin, and Seung M. Oh, J. Electrochem. Soc. **143** (7), 2204 (1996).

7 Haitao Huang, Colin A. Vincent, and Peter G. Bruce, J. Electrochem. Soc. **146** (10), 3649 (1999).

8 Ruimin Qiao, Yuesheng Wang, Paul Olalde-Velasco, Hong Li, Yong-Sheng Hu, and Wanli Yang, J. Power Sources **273**, 1120 (2015).

9 R. Benedek and M. M. Thackeray, Electrochem. Solid-State Lett. **9** (6), A265 (2006).

10 Brian L. Ellis, Kyu Tae Lee, and Linda F. Nazar, Chemistry of Materials **22** (3), 691 (2010); Brian L. Ellis, Kyu Tae Lee, and Linda F. Nazar, Chem. Mater. **22** (3), 691 (2010).

11 J. M. Tarascon, F. Coowar, G. Amatuci, F. K. Shokoohi, and D. G. Guyomard, J. Power Sources **54** (1), 103 (1995); J. M. Tarascon and D. Guyomard, Electrochim. Acta **38** (9), 1221 (1993).

12 Wanli Yang, Xiaosong Liu, Ruimin Qiao, Paul Olalde-Velasco, Jonathan D. Spear, Louis Roseguo, John X. Pepper, Yi-de Chuang, Jonathan D. Denlinger, and Zahid Hussain, J. Electron Spectrosc. Relat. Phenom. **190, Part A** (0), 64 (2013).

[13] Ruimin Qiao, Kehua Dai, Jing Mao, Tsu-Chien Weng, Dimosthenis Sokaras, Dennis Nordlund, Xiangyun Song, Vince S. Battaglia, Zahid Hussain, Gao Liu, and Wanli Yang, Nano Energy **16**, 186 (2015).
[14] Ruimin Qiao, Timothy Chin, Stephen J. Harris, Shishen Yan, and Wanli Yang, Curr. Appl. Phys. **13** (3), 544 (2013).
[15] Long Wang, Jie Song, Ruimin Qiao, L. Andrew Wray, Muhammed A. Hossain, Yi-De Chuang, Wanli Yang, Yuhao Lu, David Evans, Jong-Jan Lee, Sean Vail, Xin Zhao, Motoaki Nishijima, Seizoh Kakimoto, and John B. Goodenough, J. Am. Chem. Soc. **137** (7), 2548 (2015).
[16] Xiaosong Liu, Jun Liu, Ruimin Qiao, Yan Yu, Hong Li, Liumin Suo, Yong-sheng Hu, Yi-De Chuang, Guojiun Shu, Fangcheng Chou, Tsu-Chien Weng, Dennis Nordlund, Dimosthenis Sokaras, Yung Jui Wang, Hsin Lin, Bernardo Barbiellini, Arun Bansil, Xiangyun Song, Zhi Liu, Shishen Yan, Gao Liu, Shan Qiao, Thomas J. Richardson, David Prendergast, Zahid Hussain, Frank M. F. de Groot, and Wanli Yang, J. Am. Chem. Soc. **134** (33), 13708 (2012).
[17] Zengqing Zhuo, Jiangtao Hu, Yandong Duan, Wanli Yang, and Feng Pan, Appl. Phys. Lett. **109** (2), 023901 (2016).
[18] Ruimin Qiao, L. Andrew Wray, Jung-Hyun Kim, Nicholas P. W. Pieczonka, Stephen J. Harris, and Wanli Yang, J. Phys. Chem. C **119** (49), 27228 (2015).
[19] Xiaosong Liu, Yung Jui Wang, Bernardo Barbiellini, Hasnain Hafiz, Susmita Basak, Jun Liu, Thomas Richardson, Guojiun Shu, Fangcheng Chou, Tsu-Chien Weng, Dennis Nordlund, Dimosthenis Sokaras, Brian Moritz, Thomas P. Devereaux, Ruimin Qiao, Yi-De Chuang, Arun Bansil, Zahid Hussain, and Wanli Yang, Phys. Chem. Chem. Phys. **17** (39), 26369 (2015).
[20] Qinghao Li, Ruimin Qiao, L. Andrew Wray, Jun Chen, Zengqing Zhuo, Yanxue Chen, Shishen Yan, Feng Pan, Zahid Hussain, and Wanli Yang, J. Phys. D: Appl. Phys. **49** (41), 413003 (2016).
[21] J. J. Jia, T. A. Callcott, J. Yurkas, A. W. Ellis, F. J. Himpsel, M. G. Samant, J. Stöhr, D. L. Ederer, J. A. Carlisle, E. A. Hudson, L. J. Terminello, D. K. Shuh, and R. C. C. Perera, Rev. Sci. Instrum. **66** (2), 1394 (1995).
[22] S. Valencia, A. Gaupp, W. Gudat, Ll Abad, Ll Balcells, A. Cavallaro, B. Martínez, and F. J. Palomares, Phys. Rev. B **73** (10), 104402 (2006).
[23] G. Ghiringhelli, M. Matsubara, C. Dallera, F. Fracassi, A. Tagliaferri, N. B. Brookes, A. Kotani, and L. Braicovich, Phys. Rev. B **73** (3), 035111 (2006).
[24] James C. Hunter, J. Solid State Chem. **39** (2), 142 (1981).